RSC Advances

RSC Publishing

PAPER

View Article Online
View Journal | View Issue

Cite this: *RSC Advances*, 2013, **3**, 17300

A partially reduced C_{60}-grafted macroporous carbon composite for the enhanced electrocatalysis of nitroaromatic compounds†

Yufan Zhang, Xiangjie Bo, Charles Luhana, Huan Wang, Mian Li and Liping Guo*

Received 16th May 2013,
Accepted 22nd July 2013

DOI: 10.1039/c3ra42449a

www.rsc.org/advances

Fullerene (C_{60}) loaded in macroporous carbon (C_{60}/MPC) composite by π–π stacking was prepared and attached on a glassy carbon electrode. A novel partially reduced C_{60}-grafted MPC (K_3C_{60}/MPC) composite was fabricated when the modified electrode was subjected to cyclic voltammetric scans in KOH solution. The formation of these composite materials was verified by detailed characterization (*e.g.*, Fourier transform infrared, X-ray photoelectron spectroscopy, energy dispersive X-ray) analyses. TEM revealed that the aggregates of C_{60} with diameters of about 9.4 nm and partially reduced C_{60} moieties aggregates of ~1.8 nm in diameter were finely dispersed on the MPC surface. The resultant K_3C_{60}/MPC was used as a conductive film to significantly improve the transport of electrons and exhibited favorable electrochemical activity in terms of good stability and excellent electro-catalytic capability. More importantly, the electrochemical behavior of the as-prepared composite towards nitroaromatic compounds was assessed and a novel electrode system using linear sweep voltammetry for the preparation of an electrochemical sensor platform is proposed.

1. Introduction

Fullerene (C_{60}) possesses remarkable physicochemical properties which make it widely applied in many significant scientific and technological fields.[1–7] Electrochemistry is one of the significant fields where C_{60} is used as a mediator. C_{60} is an electron acceptor and it displays rich electrochemical properties because of its unique zero-dimensional and electronic structures. As early as 1995, Szucs *et al.* reported the immobilization of C_{60} onto electrode substrates to confer the electrocatalysis of target analytes.[8] Thereafter, L-cysteine in aqueous solution was electrochemically oxidized at a C_{60} modified glassy carbon electrode (C_{60}/GCE).[9,10] Limited work on C_{60} modified electrodes was undertaken until 2006 when Goyal and co-workers reported the electrocatalytic detection of a series of biological molecules using C_{60}/GCE.[11–17] Recently, notable works have been published for the electrochemical oxidation of carbamazepine and acyclovir at a C_{60}/GCE.[18,19] These earlier studies have shown that the C_{60}/GCE can act as an excellent working electrode due to its increased porosity and biocompatibility. Actually, the origin of the electrocatalysis is due to a partially reduced, conductive C_{60} film, rather than C_{60} itself.[14,17] Therefore, for electro-analytical applications, the C_{60}/GCE requires ''activation'', which could be achieved by reducing the C_{60} film in an aqueous solution at higher pH, typically in NaOH or KOH electrolyte to obtain conductive films.

However, single-phase materials still have limited performance because of their intrinsic weaker material properties in electronic conductivity, mechanical stability, and electrocatalytic ability. Recently, various all-carbon hybrid materials created by the functionalization of C_{60} have received intense attention, driven by the possibility of combining some of the outstanding properties of C_{60} with those of other interesting carbon materials.[5,20–28] However, the C_{60} was not in its partially reduced form in these above composite materials. This may greatly reduce the electrocatalytic ability of these composite materials, leading to their limited applications when used as electrode materials. By analogy to the aforementioned all-carbon hybrid materials, the hybridization of carbon materials with partially reduced C_{60} is envisioned to create a new class of electrode material with a strong electron-accepting capability characteristic of C_{60} and good charge transport properties.

Macroporous carbon (MPC) materials are essential for many modern applications, due to their favorable properties including strong sorbent ability for organic molecules, good thermal and mechanical stability, and excellent electrical conductivity.[29–43] Especially, the large specific surface area of MPC may offer a platform for supporting other nanoentities to form novel hybrid nanostructures with synergetic effects. Considering the excellent versatile properties of both MPC and

Faculty of Chemistry, Northeast Normal University, 130024 Changchun, P R China. E-mail: guolp078@nenu.edu.cn; Fax: +86 0431 85099762; Tel: +86 0431 85099762

† Electronic supplementary information (ESI) available. See DOI: 10.1039/c3ra42449a

C_{60}, in this study, we prepared a novel partially reduced C_{60}-grafted MPC (K_3C_{60}/MPC) material by a simple electrochemical method. This novel hybrid composite material utilized synergistic interactions between a nanostructured matrix of MPC and an excellent electron acceptor of nanosized C_{60}. To the best of our knowledge, this hybrid composite has not been reported in the previous literature. In order to investigate the applications of the K_3C_{60}/MPC composite, the electrochemical reduction of nitroaromatic compounds (NACs) was studied at the K_3C_{60}/MPC modified electrode. Moreover, K_3C_{60}/MPC can serve as an effective electrochemical sensing platform for NACs detection with high sensitivity and excellent anti-interference ability in real samples. These results indicate that this attempt provides an effective route for novel electrode material preparation and the functionalization of all-carbon materials, and is expected to significantly facilitate the design of environmental sensors.

2. Experimental

2.1 Materials

C_{60} (99.9%) was obtained from Yongxin Technology Co. Ltd. NACs, 2,4,6-trinitrotoluene (TNT), 2,4,6-trinitrophenol (TNP), nitrobenzene (NB), *o*-nitrophenol (ONP), *m*-nitrophenol (MNP), and *p*-nitrophenol (PNP) were obtained from Sigma. *N*,*N*′-dimethylformamide (DMF) (HPLC grade) and toluene were used as purchased from Beijing Chemical Co. Ltd. Toluene was refluxed for 6 h, and then distilled. The purified toluene was stored in the presence of sodium. The 0.1 M phosphate buffer solution (PBS pH 7.0), which was made up from NaH_2PO_4, Na_2HPO_4, and H_3PO_4, was employed as a supporting electrolyte. All other chemicals were at least of analytical grade. Aqueous solutions were prepared with doubly distilled water and stored in the dark.

2.2 Apparatus

All the electrochemical experiments were performed with a CHI 830B electrochemical analyzer (CH Instruments, Shanghai Chenhua Instrument Corporation, China) and a PARSTAT 2273 (AMETEK Instruments, USA) electrochemical workstation. A conventional three electrode cell was used, where the working electrode used was a GCE (model CHI104, 3 mm diameter) the modified electrode, a platinum electrode, was applied as the counter electrode and an Ag/AgCl (in saturated KCl solution) electrode served as the reference electrode. All potentials in this paper were measured and reported *versus* Ag/AgCl. In this study, all the sample solutions were purged with purified nitrogen for 20 min to remove oxygen prior to the beginning of a series of experiments and all experiments were carried out at laboratory temperature. SEM images and energy-dispersive X-ray spectra (EDX) were determined with a Philips XL-30 ESEM operating at 3.0 kV. TEM images were obtained using a JEM-2100F transmission electron microscope JEOL (Japan) operating at 200 kV. Nitrogen adsorption–desorption isotherms were measured on an ASAP 2020 Micromeritics (USA) at 77 K. The Brunauer–Emmett–Teller (BET) method was utilized to calculate the specific surface area. Fourier transform infrared (FT-IR) spectroscopy of the sample was recorded with a Nicolet Magna 560 FT-IR spectrometer with a KBr plate. X-ray photoelectron spectroscopy (XPS) was carried out using a Thermo ESCA LAB X-ray photoelectron spectrometer (USA).

2.3 Preparation of MPC

The SiO_2 template was prepared by the typical Stöber method.[44] The carbon was introduced into the interstices of the template using a modified method of Jun *et al.*[45] In a typical synthesis, 2.0 g of sucrose was dissolved in 10 mL aqueous solution containing 0.15 mL of 98% H_2SO_4. 2.0 g of SiO_2 template was immersed into sucrose solution and kept in vacuum for 3 h at room temperature for thorough impregnation. Then the mixture was heated at 100 °C for 6 h, followed by heating at 160 °C for a further 6 h for polymerization of the sucrose. The solid was subsequently carbonized at 900 °C in N_2 for 3 h in a tube oven. The SiO_2 template was then etched away by overnight dissolution in 10% aqueous HF to leave behind MPC.

2.4 Preparation of C_{60}/MPC

Firstly, 60 mg of MPC and 25 mg of C_{60} were initially suspended in 50 mL of toluene. Secondly, the mixture was subjected to ultrasound at room temperature for 3 h, in the form of 40-kHz ultrasonic waves at 100-W output power. Thirdly, the reaction mixture was washed with a large excess of toluene followed by centrifugation until the excessive precursor of C_{60} was removed. Fourth, the obtained C_{60}/MPC was dried in a vacuum oven at 60 °C for 36 h.

2.5 Preparation of K_3C_{60}/MPC

2 mg of C_{60}/MPC was dispersed into 1 mL DMF solution with ultrasonication for 30 min. After dropping 5 μL of the suspension onto the bare electrode surface, the electrode was dried in air at laboratory temperature. Finally, C_{60}/MPC/GCE was partially reduced in 1 M KOH in the potential range 0.0 to −1.5 V at 10 mV s^{-1} with a full cycle, and the K_3C_{60}/MPC/GCE was obtained after three scan cycles. For the control experiments, MPC that had not been soaked in C_{60} was subjected to cyclic voltammetric scans (CVs) and the resultant material was denoted as MPC-CVs. The preparation of K_3C_{60}/MPC is presented in Fig. 1.

3. Results and discussion

3.1 Characterization of MPC, C_{60}/MPC, and K_3C_{60}/MPC

As can be seen from the SEM (Fig. 2A) and TEM (Fig. 2B) images of the MPC, the large pores are clearly visible and the pore size is about 110 nm. The pristine MPC exhibits no

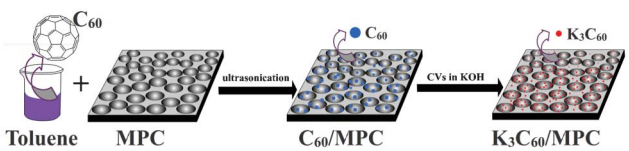

Fig. 1 Illustration of the preparation of the K_3C_{60}/MPC composite.

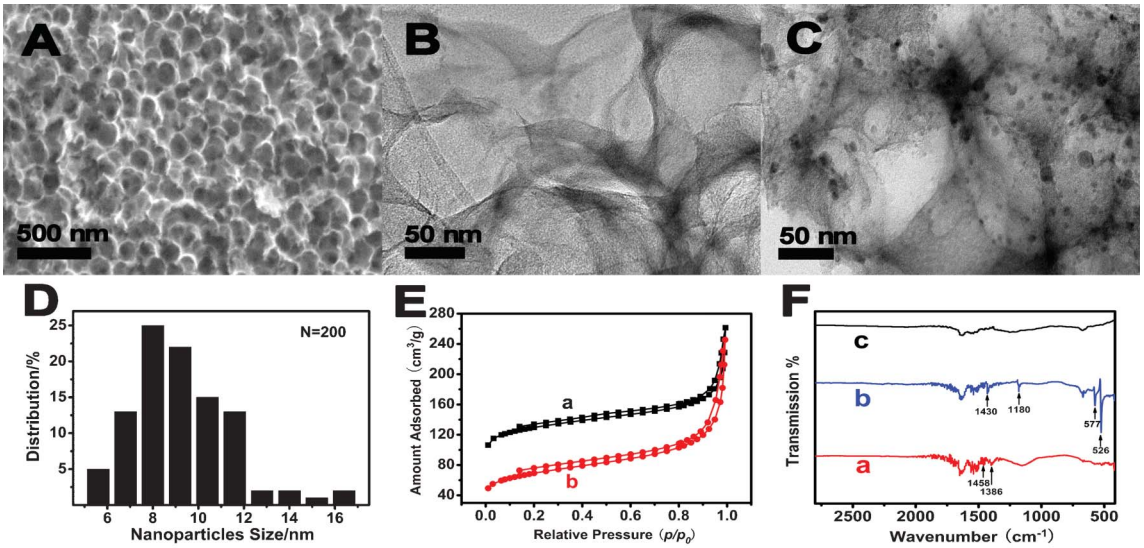

Fig. 2 (A): SEM image of MPC. (B) and (C): TEM images of MPC and C_{60}/MPC. (D): columnar distribution of C_{60} aggregates size for C_{60}/MPC. (E): Nitrogen adsorption–desorption isotherms of the MPC (curve a) and C_{60}/MPC (curve b). (F): FT-IR spectra of C_{60}/MPC (curve a), C_{60} (curve b), and MPC (curve c).

anchored nanoparticles at all (Fig. 2B). The TEM image for C_{60}/MPC given in Fig. 2C clearly displays that the MPC surface has been grafted by particles characteristic of C_{60} aggregates. As shown in Fig. 2D, the average size of C_{60} aggregates was 9.4 nm on the C_{60}/MPC. Nitrogen adsorption–desorption isotherms of the prepared MPC (curve a) and C_{60}/MPC (curve b) are presented in Fig. 2E. They contain a sharp capillary condensation step at very high relative pressures ($p/p_0 > 0.9$) and an H1-type hysteresis loop, indicating the existence of large pores in these materials.[46,47] The BET surface area and pore volume were found to decrease from 408.5 $m^2\ g^{-1}$ and 0.30 $cm^3\ g^{-1}$ for MPC to 328.0 $m^2\ g^{-1}$ and 0.26 $cm^3\ g^{-1}$ for C_{60}/MPC. The results indicate that C_{60} was loaded in MPC. Fig. 2F displays the FT-IR spectra of the C_{60}/MPC (curve a), C_{60} (curve b), and MPC (curve c). The C_{60}/MPC causes significant changes in the FT-IR spectrum of the pure C_{60} or MPC. The spectrum of bare C_{60} exhibits four clear absorptions at 526, 577, 1180, and 1430 cm^{-1}, respectively. The spectrum of C_{60}/MPC exhibits two main peaks at 1386 and 1458 cm^{-1}, which are thought to be derived from the peaks of bare C_{60} at 1180 and 1430 cm^{-1}, respectively, presumably caused by the covalent interaction between C_{60} and MPC. Further evidence for the grafting of C_{60} onto the MPC comes from XPS analysis (Fig. 3A). The oxygen/carbon atomic (O/C) ratios from XPS for MPC and C_{60}/MPC were 0.632 and 0.495, respectively. Obviously, after the functionalization of MPC using C_{60}, the relative content of oxygen containing functional groups on C_{60}/MPC decreased. This means that the C_{60} was loaded in the MPC.

After the C_{60}/MPC modified GCE (C_{60}/MPC/GCE) was subjected to CVs in KOH solution, the novel K_3C_{60}/MPC/GCE was prepared. K2*p* peaks in the spectrum of K_3C_{60}/MPC are observed in Fig. 3B, which supports the conclusion that K_3C_{60}/MPC has been successfully synthesized. However, no K peaks appeared in the spectrum of MPC-CVs. The K_3C_{60}/MPC composite was further characterized by EDX spectroscopy (Fig. 3C). The EDX spectrum of the K_3C_{60}/MPC composite shows the peaks corresponding to the C, O and K elements. For comparison, no K peak was observed for MPC-CVs. The results illustrate that the K_3C_{60}/MPC composite was prepared and the MPC was not affected by CVs in KOH solution.

The reduction of C_{60} is a multi-step transformation, which involves transient species showing ion-exchange properties. The reduction involves KC_{60}/MPC and K_2C_{60}/MPC as transient species, and the conductive K_3C_{60}/MPC as the final product. The KC_{60}/MPC and K_2C_{60}/MPC are ion-exchangers.[8] So, according to these points, we speculate the multi-step transformation as shown below:

$$C_{60}/\mathrm{MPC} \xrightarrow{-e} KC_{60}/\mathrm{MPC} \xrightarrow{-e} K_2C_{60}/\mathrm{MPC} \xrightarrow{-e} K_3C_{60}/\mathrm{MPC}$$

Fig. S1 in the ESI† indicates the C_{60}/MPC/GCE was partially reduced in 1 M KOH in the potential range 0.0 to −1.5 V at

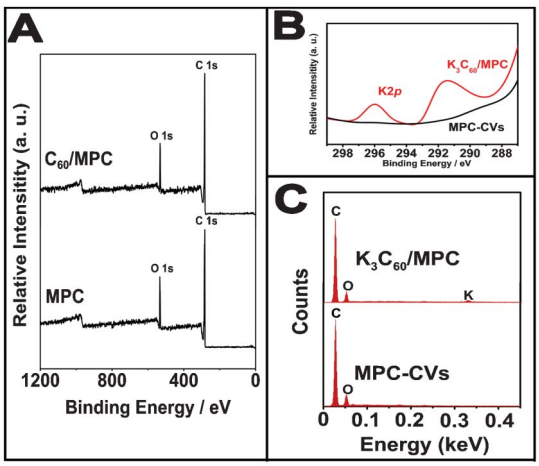

Fig. 3 (A): XPS spectra of MPC and C_{60}/MPC. (B): XPS spectra of the K2*p* region of K_3C_{60}/MPC and MPC-CVs. (C): EDX spectra of K_3C_{60}/MPC and MPC-CVs.

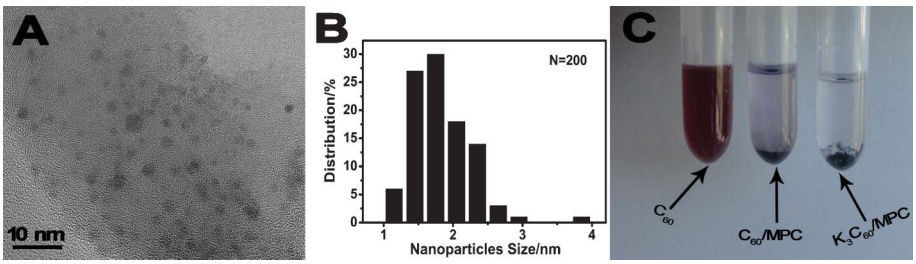

Fig. 4 (A): TEM image of K_3C_{60}/MPC. (B): columnar size distribution of C_{60} aggregates for K_3C_{60}/MPC. (C): Photographs of sample tubes containing 2.0 mg mL^{-1} of C_{60}, C_{60}/MPC and K_3C_{60}/MPC in toluene solution after ultrasonication for 8 h.

10 mV s^{-1} with a full cycle. The reduction of the films starts with a small hump at around −0.82 V. We shall call this the first reduction process. Two other smaller and broader peaks develop at around −1.12 V. We shall call these the second and third reductions, due to the two peak positions being close. This phenomenon is very similar to that reported by Szucs's group.[8]

In order to understand the role of CVs in conferring the C_{60}/MPC composite, TEM was employed to examine the surface morphologies of the C_{60}/MPC and K_3C_{60}/MPC. From the aforementioned TEM image of C_{60}/MPC (Fig. 2C), we can observe a large amount of C_{60} aggregates, and the average size of the C_{60} aggregates was 9.4 nm. However, after CVs in KOH solution, it is shown clearly that C_{60} molecules are uniformly dispersed on the MPC (Fig. 4A), and that the smaller nanoparticles of C_{60} have an average diameter of about 1.8 nm (Fig. 4B). These results are consistent with the scenario schematically shown in Fig. 1. This is because the reaction between the MPC and C_{60} originates from those sites on the surface of MPC where it is easier to take place. However, because C_{60} is more reactive than MPC, the additional free C_{60} will tend to aggregate with the C_{60} already bound on the MPC, which is susceptible to aggregation and forming C_{60} molecules clusters. Furthermore, the CVs to negative potentials provide an electron-rich environment on the MPC surface, especially at defect sites, for nucleophilic addition to the electro-deficient C_{60} to form a covalent bond. This leads to uniform dispersion of C_{60} on the MPC surface. This phenomenon is very similar to the literature.[20] Significantly, it does not only make the C_{60} partially reduced, but also leads to uniform dispersion of C_{60} on the MPC surfaces. Conceivably, these two factors may jointly enhance the electro-catalytic ability of the K_3C_{60}/MPC.

Moreover, due to stronger interactions between the partially reduced C_{60} and MPC, the obtained composite is more stable. For the sake of better evidence of more stability of the K_3C_{60}/MPC composite, C_{60}/MPC and K_3C_{60}/MPC were taken into toluene solution and subjected to ultrasonication for 8 h. Fig. 4C depicts the toluene solution of C_{60}/MPC and K_3C_{60}/MPC mixtures after ultrasonication, and the same amount of pure C_{60} was also dissolved in toluene solution. It is clearly observed that the toluene solution turns purple, a characteristic color of C_{60}, which indicates that the C_{60} was separated from the C_{60}/MPC, and dissolved into the toluene solution. However, the color of the toluene solution remained unchanged in the K_3C_{60}/MPC suspension. This demonstrated that the K_3C_{60}/MPC composite is more stable. This is because in the synthetic procedure of C_{60}/MPC, C_{60} attaches to the MPC with π–π stacking, whereas the K_3C_{60}/MPC involves stronger covalent interactions between MPC and C_{60} induced by the CVs.

3.2 Electrochemical behavior of K_3C_{60}/MPC/GCE

Electrochemical impedance spectroscopy (EIS) was applied to analyze the electronic conductivity of different electrode materials (Fig. 5A). The sequence of the values of charge-

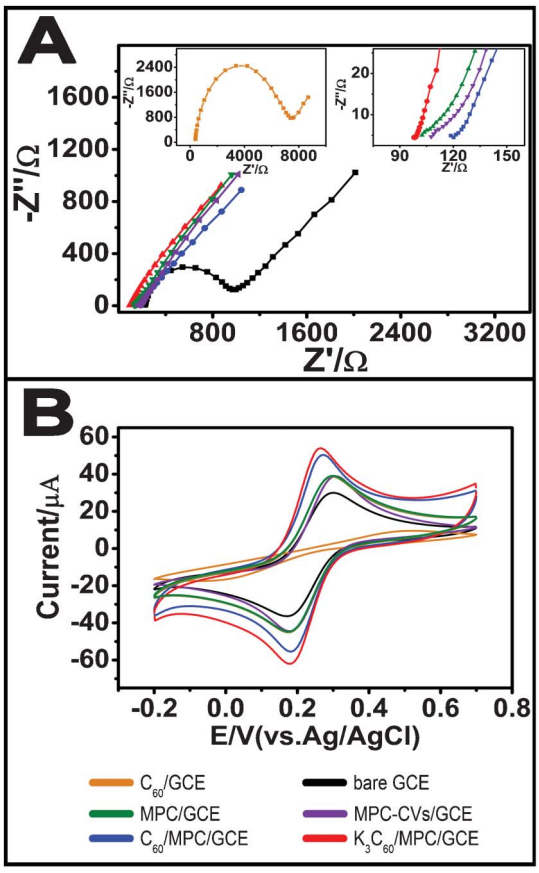

Fig. 5 (A): EIS results of different electrodes in a 0.1 M KCl solution containing 5.0 mM $K_3Fe(CN)_6/K_2Fe(CN)_6$ and from 0.1 Hz to 10.0 KHz. (B): Background-corrected CV for $K_3Fe(CN)_6/K_2Fe(CN)_6$ solution at different electrodes. Scan rate, 50 mV s^{-1}.

transfer resistance (R_{ct}) for the different electrodes is C_{60}/GCE > bare GCE > MPC/GCE ~ MPC-CVs/GCE > C_{60}/MPC/GC > K_3C_{60}/MPC/GC (for five determinations). The detailed data is shown in Table S1, ESI.† This result indicates that the K_3C_{60}/MPC makes the electron transfer easier than with other modifiers. Fig. 5B depicts the background-corrected CV for different electrodes in 5 mM $K_3Fe(CN)_6/K_2Fe(CN)_6$ solution at a scan rate of 50 mV s^{-1}. Table S1, ESI† displays the peak currents (I_p) and peak separations (ΔE_p) of the electrodes. The results show that the largest value of I_p and the smallest ΔE_p are observed at the K_3C_{60}/MPC/GCE, which may exhibit the best electrochemical reaction ability among them. In the neutral state, C_{60} on the electrode surface may serve to act as inert particles and mass transfer blocking layer, thus, hindering the diffusion of the electro-active species to the electrode surface, which appears to slow down the rate of electron transfer.[19] Nevertheless, in the case of C_{60} in the C_{60}/MPC, C_{60} can be regarded as an excellent electron acceptor and its conjugation with a conductive matrix of MPC forms a unique hetero-structure.[20] Additionally, the dispersion of nanosized C_{60} on the surface of MPC with large surface area may offer a microenvironment for transferring species in solution through the pores of C_{60}/MPC, which would be beneficial for accelerating heterogeneous electron transfer between the electrode and species in solution.[21] Furthermore, the C_{60}/MPC can be partially reduced electrochemically in KOH aqueous solutions, forming conductive films with more electrocatalytic ability.

3.3 Electrochemical detection of NACs by the K_3C_{60}/MPC/GCE

NACs are known for their detrimental effects on the environment and human health as toxic and mutagenic substances.[48–50] Therefore, the needs of public security and environmental protection accelerate the research and development efforts to detect NACs. As a further significant step, in order to investigate the applications of K_3C_{60}/MPC composite, this novel electrode material was used as an electrochemical sensor for NACs, such as TNT, TNP, NB, ONP, MNP, and PNP. The performance of different electrodes for analysing NACs was investigated by linear sweep voltammetry (LSV) (Fig. 6). Clearly, as compared to other electrodes, lower over-voltages for reduction potentials, as well as larger peak currents, were achieved at K_3C_{60}/MPC/GCE. Furthermore, various current responses for NACs at the MPC/GCE, C_{60}/MPC/GCE, and K_3C_{60}/MPC/GCE are depicted in Fig. S2, ESI,† and the detailed data of linear range, detection limit, and sensitivity for NACs are given in Table S2, ESI.† The results also exhibit the best electrochemical parameters for NACs obtained at the K_3C_{60}/MPC/GCE. The greatly enhanced electrochemical activity of the K_3C_{60}/MPC can be explained by the following synergy hypothesis: the high specific surface area of MPC, which acts as a good support platform, and the electron acceptor of C_{60} could improve the electronic transport capacity of the composite. Additionally, the C_{60}/MPC requires ''activation'' which could be achieved by reducing the C_{60}/MPC film in an aqueous solution at a higher pH. So, the electro-catalytic ability of K_3C_{60}/MPC could be improved, and the promoted charge propagation through the K_3C_{60}/MPC/GCE facilitates the reaction between NACs and the electrode surface.

3.4 Repeatability, stability and interference

Based on its favorable electrochemical properties, the K_3C_{60}/MPC can be used as a novel electrode material to explore electro-analytical applications. So the repeatability and stability studies of K_3C_{60}/MPC/GCE are necessary. The repeatability

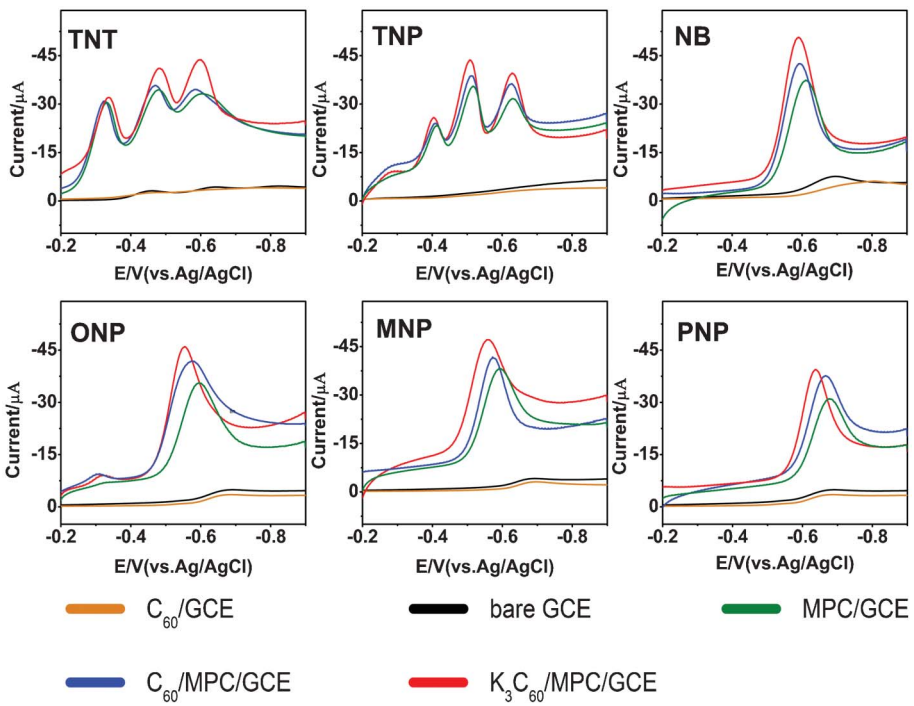

Fig. 6 LSV for 100 μM TNT, TNP, NB, ONP, MNP, and PNP at different electrodes. Electrolyte, 0.1 mol L^{-1} pH 7.0 PBS. Scan rate, 50 mV s^{-1}.

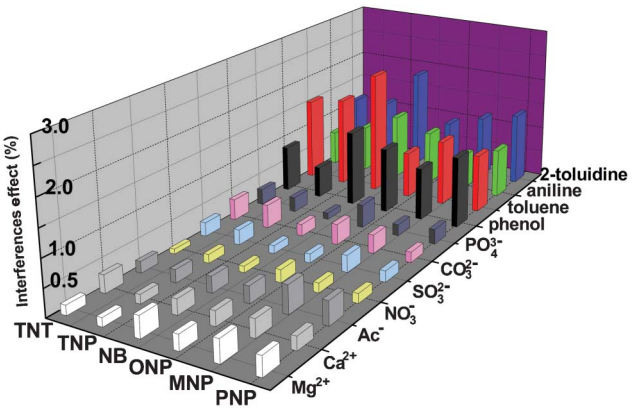

Fig. 7 Normalized current of K_3C_{60}/MPC/GCE for 50 μM NACs in the presence of the high concentrations of possible interferents.

of the sensor was studied by performing parallel experiments. The relative standard deviation (RSD) of the sensitivity was less than 6.3% (n = 5). When not in use, the K_3C_{60}/MPC/GCE was stored under dry conditions at 4 °C for three weeks. The results show that, the current response to 100 μM NACs retained more than 90.7% of its original value, reflecting the good long-term stability of the electrode.

Possible interferences for the detection of NACs at the K_3C_{60}/MPC/GCE were also investigated by addition of various inorganic ions and organic pollutants (Fig. 7). The results show that the determination of 50 μM NACs could not be affected by a 100-fold increase of Mg^{2+}, Ca^{2+}, Ac^-, NO_3^-, SO_4^{2-}, CO_3^{2-}, and PO_4^{3-} at the K_3C_{60}/MPC/GCE. The interference of organic compounds, namely phenol, toluene, aniline, and 2-toluidine were also tested under the optimized experimental conditions. A little response to these organic compounds was found when their concentrations were 10-fold higher than the NACs in this potential range. This implies that the K_3C_{60}/MPC/GCE has excellent anti-interference ability and may have promising application for NACs assay in real water samples.

3.5 Analysis of NACs in real samples

In order to evaluate the practical application of this fabricated electrode, the determination of NACs in lake water by LSV (10 mV s^{-1}) was recorded. The standard addition method was applied to estimate the reliability at three concentration levels in recovery tests. The analytical results obtained are summarized in Table S3, ESI.† The average recoveries ranged between 94.8 and 109.0%, with the RSDs less than 5.0% (n = 5). This demonstrates that the novel K_3C_{60}/MPC/GCE is practical for the determination of NACs in environmental samples.

4. Conclusions

We have developed an easy strategy for producing partially reduced C_{60}-grafted MPC. Detailed characterization analyses confirm that the K_3C_{60}/MPC composite was successfully synthesized. TEM observation reveals the partially reduced C_{60} moieties aggregates of ~1.8 nm in diameter with fine dispersion on the MPC surface. The electrochemical results indicate that the resultant K_3C_{60}/MPC is an excellent electron accepting/charge transporting composite for constructing efficient electrode materials. Also, as a novel electrode material, K_3C_{60}/MPC possesses favorable electrochemical activity, good stability, and excellent electro-catalytic properties. As a further significant step, K_3C_{60}/MPC can serve as a novel, effective, electrochemical sensing platform for NACs detection with excellent anti-interference ability in real samples. The study of the K_3C_{60}/MPC system in this work is not only a good example for constructing a promising electrochemical sensing platform for the detection of NACs, but also should be a good model for the further design and investigation of fullerene-carbon derivative hybrid materials for the potential applications of environmental pollutant sensors.

Acknowledgements

The authors gratefully acknowledge the financial support of the National Natural Science Foundation of China (No. 21075014), the State Key Laboratory of Electroanalytical Chemistry, CIAC, CAS (No. SKLEAC201201) and the Fundamental Research Funds for the Central Universities (No. 12SSXT145).

References

1 H. C. Wong, A. M. Higgins, A. R. Wildes, J. F. Douglas and J. T. Cabral, *Adv. Mater.*, 2013, **25**, 985–91.
2 S. Urnikaite, T. Malinauskas, V. Gaidelis, R. Maldzius, V. Jankauskas and V. Getautis, *Carbon*, 2011, **49**, 320–325.
3 C. Gu, Z. Zhang, S. Sun, Y. Pan, C. Zhong, Y. Lv, M. Li, K. Ariga, F. Huang and Y. Ma, *Adv. Mater.*, 2012, **24**, 5727–5731.
4 J. A. Rather and K. De Wael, *Sens. Actuators, B*, 2013, **176**, 110–117.
5 L. Xiao, G. G. Wildgoose, A. Crossley and R. G. Compton, *Sens. Actuators, B*, 2009, **138**, 397–401.
6 L. Chen, K. Yao and Y. Chen, *J. Mater. Chem.*, 2012, **22**, 18768–18771.
7 T. Ichiki, Y. Matsuo and E. Nakamura, *Chem. Commun.*, 2013, **49**, 279–281.
8 A. Szucs, A. Loix, J. B. Nagy and L. Lamberts, *J. Electroanal. Chem.*, 1995, **397**, 191–203.
9 W. T. Tan, A. M. Bond, S. W. Ngooi, E. B. Lim and J. K. Goh, *Anal. Chim. Acta*, 2003, **491**, 181–191.
10 R. T. Kachoosangi, C. E. Banks and R. G. Compton, *Anal. Chim. Acta*, 2006, **566**, 1–4.
11 R. N. Goyal, V. K. Gupta, A. Sangal and N. Bachheti, *Electroanalysis*, 2005, **17**, 2217–2223.
12 R. N. Goyal and S. P. Singh, *Electrochim. Acta*, 2006, **51**, 3008–3012.
13 R. N. Goyal and S. P. Singh, *Talanta*, 2006, **69**, 932–937.
14 R. N. Goyal, N. Bachheti, A. Tyagi and A. K. Pandey, *Anal. Chim. Acta*, 2007, **605**, 34–40.

15 R. N. Goyal, V. K. Gupta and N. Bachheti, *Anal. Chim. Acta*, 2007, **597**, 82–89.
16 R. N. Goyal, V. K. Gupta, M. Oyama and N. Bachheti, *Talanta*, 2007, **71**, 1110–1117.
17 R. N. Goyal, D. Kaur, S. P. Singh and A. K. Pandey, *Talanta*, 2008, **75**, 63–69.
18 S. S. Kalanur, S. Jaldappagari and S. Balakrishnan, *Electrochim. Acta*, 2011, **56**, 5295–5301.
19 N. P. Shetti, S. J. Malode and S. T. Nandibewoor, *Bioelectrochemistry*, 2012, **88**, 76–83.
20 H. Zhang, L. Fan, Y. Fang and S. Yang, *Chem. Phys. Lett.*, 2005, **413**, 346–350.
21 M. Zhou, J. Guo, L. P. Guo and J. Bai, *Anal. Chem.*, 2008, **80**, 4642–4650.
22 S. Gorantla, S. Avdoshenko, F. Börrnert, A. Bachmatiuk, M. Dimitrakopoulou, F. Schäffel, R. Schönfelder, J. Thomas, T. Gemming, J. H. Warner, G. Cuniberti, J. Eckert, B. Büchner and M. H. Rümmeli, *Nano Res.*, 2010, **3**, 92–97.
23 J. Yang, M. Heo, H. J. Lee, S. M. Park, J. Y. Kim and H. S. Shin, *ACS Nano*, 2011, **5**, 8365–8371.
24 Y. Yi, W. M. Choi, B. Son, J. W. Kim and S. J. Kang, *Carbon*, 2011, **49**, 4936–4839.
25 Y. Zhang, L. Ren, S. Wang, A. Marathe, J. Chaudhuri and G. Li, *J. Mater. Chem.*, 2011, **21**, 5386–5391.
26 D. J. Bindl, A. S. Brewer and M. S. Arnold, *Nano Res.*, 2011, **4**, 1174–1179.
27 J. A. Rather and K. De Wael, *Sens. Actuators, B*, 2012, **171–172**, 907–915.
28 N. Mackiewicz, T. Bark, B. Cao, J. A. Delaire, D. Riehl, W. L. Ling, S. Foillard and E. Doris, *Carbon*, 2011, **49**, 3998–4003.
29 K. T. Lee, J. C. Lytle, N. S. Ergang, S. M. Oh and A. Stein, *Adv. Funct. Mater.*, 2005, **15**, 547–556.
30 J. Hu, H. Wang, Q. Gao and H. Guo, *Carbon*, 2010, **48**, 3599–3606.
31 C. Huang, R. Dong, D. Gu and D. Zhao, *Carbon*, 2011, **49**, 3055–3064.
32 W. Huang, H. Zhang, Y. Huang, W. Wang and S. Wei, *Carbon*, 2011, **49**, 838–843.
33 J. Balach, M. M. Bruno, N. G. Cotella, D. F. Acevedo and C. A. Barbero, *J. Power Sources*, 2012, **199**, 386–394.
34 Y. Han, X. Dong, C. Zhang and S. Liu, *J. Power Sources*, 2012, **211**, 92–96.
35 Y. Hu, Z. Wen, X. Wu and J. Jin, *J. Power Sources*, 2012, **219**, 1–8.
36 L. Jia, G. P. Mane, C. Anand, D. S. Dhawale, Q. Ji, K. Ariga and A. Vinu, *Chem. Commun.*, 2012, **48**, 9029–9031.
37 J. Liang, Y. Zheng, J. Chen, J. Liu, D. Hulicova-Jurcakova, M. Jaroniec and S. Z. Qiao, *Angew. Chem., Int. Ed.*, 2012, **51**, 3892–3896.
38 S. Lu and Y. Liu, *Appl. Catal., B*, 2012, **111–112**, 492–501.
39 Y. Lv, L. Gan, M. Liu, W. Xiong, Z. Xu, D. Zhu and D. S. Wright, *J. Power Sources*, 2012, **209**, 152–157.
40 A. Walcarius, *TrAC, Trends Anal. Chem.*, 2012, **38**, 79–97.
41 G. Yang, H. Han, T. Li and C. Du, *Carbon*, 2012, **50**, 3753–3765.
42 T. Zhang, C. Z. Lai, M. A. Fierke, A. Stein and P. Buhlmann, *Anal. Chem.*, 2012, **84**, 7771–7778.
43 G. Lalwani, A. T. Kwaczala, S. Kanakia, S. C. Patel, S. Judex and B. Sitharaman, *Carbon*, 2013, **53**, 90–100.
44 W. Stöber, A. Fink and E. Bohn, *J. Colloid Interface Sci.*, 1968, **26**, 62–69.
45 S. Jun, J. Sang Hoon, R. Ryoo, M. Kruk, M. Jaroniec, Z. Liu, T. Ohsuna and O. Terasaki, *J. Am. Chem. Soc.*, 2000, **122**, 10712–10713.
46 W. Li, D. Chen, Z. Li, Y. Shi, Y. Wan, G. Wang, Z. Jiang and D. Zhao, *Carbon*, 2007, **45**, 1757–1763.
47 Y. F. Zhang, L. J. Zeng, X. J. Bo, H. Wang and L. P. Guo, *Anal. Chim. Acta*, 2012, **752**, 45–52.
48 K. Ayoub, E. D. van Hullebusch, M. Cassir and A. Bermond, *J. Hazard. Mater.*, 2010, **178**, 10–28.
49 M. Sui, J. Liu and L. Sheng, *Appl. Catal. B: Environ.*, 2011, **106**, 195–203.
50 X. Chen, X. Cheng and J. J. Gooding, *Anal. Chem.*, 2012, **84**, 8557–8563.

